Nanocrystalline cobalt–nickel–boron (metal boride) catalysts for efficient hydrogen production from the hydrolysis of sodium borohydride

Aybike Paksoy[1†], Samira Fatma Kurtoğlu[2,3†], Azam Khodadadi Dizaji[2,3], Zerrin Altıntaş[1], Sina Khoshsima[1], Alper Uzun[2,3,4], Özge Balcı[1,5*]

[1]*Koç University Boron and Advanced Materials Application and Research Center (KUBAM), Rumelifeneri Yolu, Sarıyer, 34450, İstanbul, Turkey*

[2]*Koç University TÜPRAŞ Energy Center (KUTEM), Rumelifeneri Yolu, Sarıyer, 34450, İstanbul, Turkey*

[3]*Koç University, Department of Chemical and Biological Engineering, Rumelifeneri Yolu, Sarıyer, 34450, İstanbul, Turkey*

[4]*Koç University Surface Science and Technology Center (KUYTAM), Koç University, Rumelifeneri Yolu, Sariyer, 34450, Istanbul, Turkey*

[5]*Koç University, Department of Chemistry, Rumelifeneri Yolu, Sarıyer, 34450, İstanbul, Turkey*

**Corresponding Author: E-mail: obalci@ku.edu.tr, Phone: +90 212 338 1566*

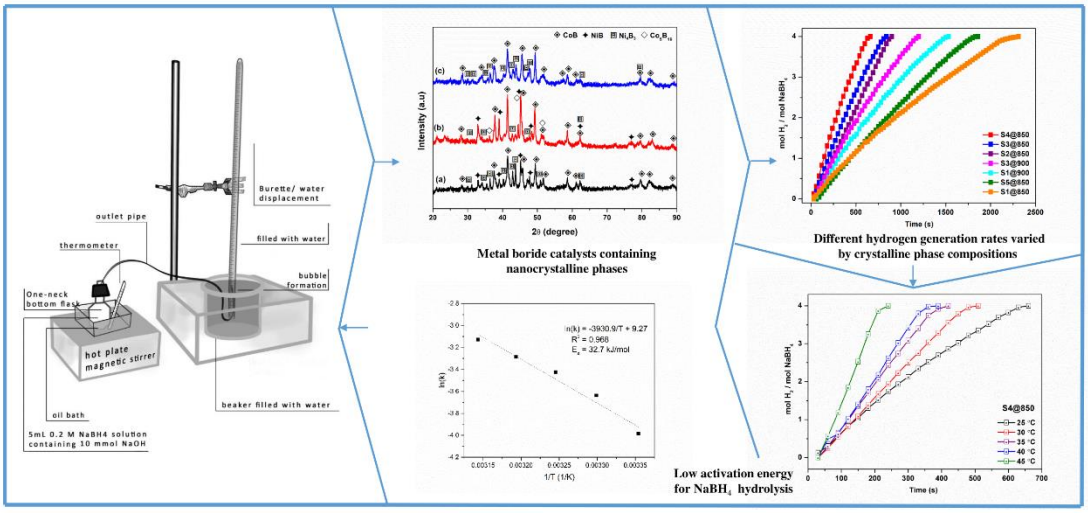
†These authors contributed equally to this work.

Abstract

Innovative metal boride nanocatalysts containing crystalline Co–Ni based binary/ternary boride phases were synthesized and used in the hydrolysis of $NaBH_4$. All the as-prepared catalysts were in high-purity with average particle sizes ranging between ~51 to 94 nm and consisting of different crystalline phases (e.g. CoB, Co_2B, Co_5B_{16}, NiB, Ni_4B_3, $Ni_2Co_{0.67}B_{0.33}$). The synergetic effect of the different binary/ternary boride phases in the composite catalysts had a positive role on the catalytic performances thus, while the binary boride containing phases of unstable cobalt borides or single Ni_4B_3 were not showing any catalytic activity. The Co–Ni–B based catalyst containing crystalline phases of CoB–Ni_4B_3 exhibited the highest H_2 production rate (500.0 ml H_2 min^{-1} g_{cat}^{-1}), with an apparent activation energy of 32.7 kJ/mol. The

recyclability evaluations showed that the catalyst provides stability even after the 5th cycle. The results suggested that the composite structures demonstrate favorable catalytic properties compared to those of their single components and they can be used as alternative and stable catalysts for efficient hydrogen production from sodium borohydride.

Graphical Abstract



Keywords: Cobalt boride, nickel boride, nanocrystalline particles, composite catalyst, sodium borohydride, hydrolysis

Abbreviations:

XRD: X-Ray Diffractometer

FE-SEM: Field Emission Scanning Electron Microscope

DLS: Dynamic Light Scattering

EDX: Energy-Dispersive X-Ray Spectroscopy

MA'd: Mechanically Alloyed

XRF: X-Ray Fluorescence Spectrometer

ICDD: The International Center for Diffraction Data

SI: Supporting Information

CP: Commercial Powder

CNT: Carbon Nano-Tube

1. Introduction

Hydrogen is a potential material that satisfies the increasing demand for efficient and clean energy sources, and so this can be seen as a clean and sustainable energy carrier in the transition from fossil fuels to renewable energy sources. Thus, highly efficient hydrogen release and storage methods have attracted much attention worldwide [1]. In the past few years, complex hydrides have been proven as promising hydrogen sources for carrier application [2]. However, safe storage and efficient release of hydrogen in ambient conditions remains a major obstacle for its widespread use. Recently, more efforts have been made to discover hydrogen storage materials. Among the hydrides, sodium borohydride ($NaBH_4$) stands out due to its high theoretical hydrogen content of 10.8 wt.%, nontoxicity, excellent stability of its solution at room temperature under high pH value and harmless product ($NaB(OH)_4$) of the hydrolysis reaction [3–5]. Regarding these properties, sodium borohydride can be considered as a material that safely produces a significant amount of hydrogen when undergoing the hydrolysis reaction.

High-purity-hydrogen can be controllably released from the hydrolysis of $NaBH_4$ alkaline solution in the presence of certain catalysts [1,2,6]. The activation energy of the sodium borohydride hydrolysis reaction carried out without using any catalyst is known to be 217 kJ/mol, which is significantly higher compared to the activation energy measured when a catalyst is present [1]. Under these conditions, the hydrogen production performance of the hydrolysis of $NaBH_4$ is not sufficient to meet the quantity demand [4]. For example, as can be determined from the studies of Zhao et al. and Liang et al, the use of catalysts consisting of Ni–B and Co–B particles, respectively, reduced the activation energy of the sodium borohydride hydrolysis reaction to 57.8 and 72.52 kJ/mol [7,8]. As can be demonstrated from these values, the use of catalysts can decrease the activation energy by almost four-times. Therefore, the choice of catalyst is the key factor affecting the hydrogen production performance for the

hydrolysis of $NaBH_4$ [7]. In addition, this reaction produces $NaBO_2$ as a by-product and this has two advantages: $NaBO_2$ can be converted to $NaBH_4$ and also it is non-toxic [9]. Traditionally known catalysts are noble metal catalysts such as Pt-, Ir-, Pd-, Rh-, and Ru-based ones. While these noble-metal-based catalysts provide high activity in all environments including acidic and alkaline environments, they can also maintain their chemical stability. However, they are very expensive due to their rarity which is a major disadvantage and that limits commercialization [10]. Recently, to obtain pure hydrogen, some non-noble metals and their alloys have been identified to catalyze the hydrolysis of $NaBH_4$, including $LaNi_{4.5}T_{0.5}$ (T = Mn, Cr, Co, Fe, Cu, Al), nickel and cobalt, nickel boride and cobalt boride [11–13]. Among the mentioned transition metals, cobalt and nickel are one of the most remarkable ones. While cobalt is outstanding because of its low cost, superior stability, and activity, nickel compounds such as NiB, Ni_2B, and Ni_3B have been known as multistranded materials with potential applications in hydrogen production, oxygen evolution, and water splitting [14,15]. Especially under optimized pH environments, different borides, such as MoB, NiB, CoNiB have been found to exhibit favorable catalytic performances for the hydrogen evolution reaction [16]. However, non-noble metal catalysts normally provide relatively low activity compared to noble-metal catalysts. Therefore, improving the hydrogen production rate of the non-noble-metal based catalysts has become a necessary task.

Since the activity of a catalyst is directly related to the particle size and degree of dispersion, small particle size and well-dispersed catalysts may cause sufficient contact with the reagent; which is very important in enhancing the reaction rate and saving catalyst quantitatively [7,17]. Thus, use of a support material with a large surface area provides a potential solution, which also means an additional processing step. There are studies in the literature on the use of non-supported Co-based binary and ternary metal boride compounds as catalysts in the hydrogen storage and fuel cell technology, thus Co–B compounds were used to study catalytic

performance for the hydrolysis of $NaBH_4$. In these studies, it has been proved that cobalt borides (CoB, $Co_{2.0-3.3}B$, Co_3B) and Co–B alloys in different stoichiometry significantly increase the catalytic performance for the hydrogen generation by $NaBH_4$ [7,12,18]. In similar studies, it was observed that addition of a metal to metal boride compounds or alloys significantly increases the catalytic performance [19]. The properties such as wider active surface area and the improved absorption ability in the ternary phases were obtained with a second metal addition, which has made the metal–metal–boron ternary systems to be more desirable in the catalytic filed [19]. The matching electronic interaction between Co, Ni and Fe metals has caused these metal combinations to be used to develop ternary boride alloys. In this regard, the catalytic effect of amorphous alloys of the Co–Ni–B system in various solutions has been extensively studied in the literature [17,20–25]. The presence of additional third elements such as iron in the structure of cobalt boride (Co–Fe–B) compounds is reported to complement and enhance the properties of the mentioned surfaces by providing greater surface area and improved catalytic activity compared to binary borides [19,26,27]. It was concluded that this increase in activity is due to the high Co–B dispersion and electron transfer from B and Fe atoms to Co active regions in addition to large surface area [28]. In all of these studies, binary and ternary boride compounds or alloys, chloride salts and the final products that are obtained by the reaction of a chemical reducer in an aqueous or organic environment are amorphous [17,19–25]. There are few studies in the literature where amorphous Co–Ni–B catalysts are used in the hydrolysis of $NaBH_4$ [7,17]. However, it is known that obtaining these alloys in crystalline form or in smaller nanoparticle sizes, would greatly increase the catalytic performance [12]. In a previous study that analyzed the catalytic effect of $Co_{1-x}Ni_xB$ alloys during $NaBH_4$ hydrolysis, it was determined that the maximum hydrogen generation rate was reached when $x = 0.15$ [29]. There are few studies in the literature that discussed the synthesis and catalytic performance of Co-based ternary boride particles especially when they are crystalline rather than in their

amorphous state [30]. Generally, transition metal borides have the desirable attributes such as low synthesis cost, easy processing, and metal-like conductivity which makes them interesting materials [16].

In the present study, the preparation of innovative binary/ternary composite metal borides that are aimed in crystalline form with fine grain sizes, and high chemical stability are therefore considered to be very suitable for use as catalysts. Synthesis methods of crystalline and nanoscale cobalt-nickel metal boride catalysts are much less known than their binary compounds or amorphous structures, and are still being investigated. The present work reports the one-step synthesis of nanocrystalline cobalt-nickel-boron-based metal boride catalysts with their corresponding catalytic performance tests, and explains the evolution of catalytic activities on the sodium borohydride hydrolysis reaction. In order to characterize the synthesized metal borides, XRD/XRF analyses, FE-SEM/EDX analyses, and DLS particle size measurements are added to the study. In addition to measure catalytic performance, recyclability results are also included. Considering the microstructural and chemical analysis of the nanocrystalline Co–Ni–B based compounds, the development of these materials towards desirable product applications as catalysts would be feasible.

2. Experimental Procedure

2.1. Preparation and analysis of the catalysts

In order to synthesize the catalyst nanoparticles, the anhydrous cobalt chloride ($CoCl_2$, Alfa Aesar, 99.7 % purity) and nickel chloride ($NiCl_2$, Alfa Aesar, 99 % purity) powders as the metal chlorides and sodium borohydride ($NaBH_4$, Alfa Aesar, 98% purity) as the boron source were used in the experiments. To induce the reaction through the liquid phase and to avoid loss of products in the gaseous phase, the reaction was carried out in an inorganic molten salt medium. Thus, to carry out the reaction in liquid phase, the LiCl/KCl eutectic mixture (45:55 wt. %) was used as a water-soluble and low-melting-point inorganic salt solvent [31,32].

The amounts of $CoCl_2$–$NiCl_2$–$NaBH_4$ mixtures were calculated based on the theoretical reaction between the precursors thereby accounting for the mole ratio of metal chlorides to $NaBH_4$ as 1:3 and 1:6, which results in $CoNiB_{x(s)}$, $NaCl_{(s)}$ and $H_{2(g)}$ as the reaction products, in order to prepare the ternary Co–Ni–B catalysts [33,34]. Thus, 1 mole of $CoCl_2$ and $NiCl_2$ were added for a 1-gram ternary system, while $NaBH_4$ was added at ratios of 3 or 6 moles. For comparison purposes, the synthesis of binary borides was also studied by using the $CoCl_2$–$NaBH_4$ or $NiCl_2$–$NaBH_4$ mixtures based on a mole ratio of metal chlorides to $NaBH_4$ as 1:6. Thus, $CoCl_2$ or $NiCl_2$ was used at the ratio of 1 mole in a total sample of 1 gram, while $NaBH_4$ was added at the ratio of 6 moles.

The amount of the eutectic mixture was 10 times of the total amount of the precursor powders. All the preparation and handling steps were carried out under Ar atmosphere in an MBraun™ glove box. To obtain a homogenous mixture, the precursors were introduced to a short-time ball mill process, which was carried out for 3 min using a Retsch™ PM100 planetary ball mill with a rate of 600 rpm and a ball-to-powder weight ratio (BPR) of 4:1. Only one set of the mixtures were mechanically alloyed (MA'd) for 2 min using a Spex™ 8000D high energy ball mill with a rate of 1200 rpm and a BPR of 4:1. Milling vials and balls made of hardened steel were used during the milling processes of precursors.

The mixtures were then introduced into a 316-L stainless steel tube and sealed via Ar welding. All the reactions were carried out under autogenic pressure in a sealed tube that was placed in a Protherm™ chamber furnace. The powders were heated up to 850 and 900°C, and then kept at that temperature for a duration of 2 h to obtain the nanocrystalline particles.

All the as-synthesized powders were leached with hot distilled water using an ultrasonic bath for 15 min, for the elimination of NaCl by-product and unreacted eutectic mixture. The leached solution was then introduced to a Sigma centrifuge device for precipitation of the powders at 3500 rpm for a duration of 15 min. The obtained solution was dumped, and precipitated powder

was extracted and dried overnight under vacuum at 70 °C. Table 1 summarizes the synthesis conditions and their corresponding sample names for Co–Ni–B catalysts. For comparison purposes, the commercially available cobalt boride powder (Co_2B–Co_3B, Alfa Aesar, 99 % purity) was also used as a catalyst, and is named as CP, as seen in Table 1.

Table 1. Synthesis conditions for Co–Ni–B, Co–B and Ni–B catalysts.

Sample Name	Synthesis conditions		
	Starting powders	**Ratio of metal chlorides to $NaBH_4$ (mole)**	**Reaction Temperature (°C)**
S1@850	$CoCl_2$–$NiCl_2$–$NaBH_4$	1:3	850
S1@900	$CoCl_2$–$NiCl_2$–$NaBH_4$	1:3	900
S2@850	$CoCl_2$–$NiCl_2$–$NaBH_4$ (+2 mole of B)	1:3	850
S3@850	$CoCl_2$–$NiCl_2$–$NaBH_4$	1:6	850
S3@900	$CoCl_2$–$NiCl_2$–$NaBH_4$	1:6	900
S4@850	$CoCl_2$–$NiCl_2$–$NaBH_4$ (MA'd for 2 min)	1:6	850
S5@850	$CoCl_2$–$NaBH_4$	1:6	850
S6@850	$NiCl_2$–$NaBH_4$	1:6	850
CP	*commercially available powder*		

Phase analysis was conducted using a Rigaku™ Miniflex600 Series X-ray diffractometer (XRD) with CuK_α radiation at a scan rate of 10°/min and a step size of 0.02°. *XRF reduction* mode of the device was conducted by changing the detector angle in order to reduce the fluorescence effect of Co. The International Center for Diffraction Data (ICDD) powder diffraction files were used to determine the crystalline phases. The microstructures were investigated using a Zeiss™ Ultra Plus Field Emission Scanning Electron Microscope (FE-SEM); and the secondary electron detector was used to obtain the images (at 3 and 5 kV of acceleration voltages) by setting the working distance at about 3.5-5.5 mm. Bruker XFlash 5010 energy dispersive X-Ray spectrometer (EDS) detector with 123 eV resolution was used for EDX analysis to obtain the elemental mapping of the samples on the selected area. Average particle sizes were calculated from the FE-SEM images taken at different magnifications: The result of each sample represents the arithmetic mean of twenty measurements of particle sizes

and its standard deviation. Particle size distribution graphs were obtained by using a Malvern™ Zetasizer dynamic light scattering (DLS). Chemical analyses of the powders were conducted using a Bruker™ S8 TIGER X-ray fluorescence spectrometer (XRF), and the elemental composition up to ppm level (except elemental boron, which is not under limit of the device) was reported as wt. % of the total amount.

2.2. Hydrolysis of $NaBH_4$

The catalytic performance of the synthesized particles was investigated for hydrogen production from the $NaBH_4$ solution. The catalytic performance measurements were made by charging the $NaBH_4$ solution and catalysts into reactors, and then measuring the amount of hydrogen that is released over time. The measured hydrogen production rates were then evaluated in the light of differences in catalyst structures, and the effects of structural differences on catalytic performance were revealed.

Figure 1 shows the experimental setup for hydrogen generation from the hydrolysis of $NaBH_4$ that was used for catalytic performance measurements. To conduct catalytic activity measurement experiments, 5 mL of 0.2 M $NaBH_4$ solution containing 10 mmol NaOH was placed in a closed one-neck round bottom flask with an outlet tube for collecting the released hydrogen gas. The hydrostatic pressure formed due to the presence of the water in the burette, and the vapor pressure of water were neglected and the total pressure of the H_2 collected was assumed constant throughout the experiment at the atmospheric pressure. A comparison of the volume of hydrogen generated by taking these into considerations and by neglecting them is presented in Figure S1, in the Supporting Information (SI). According to Figure S1, data show that the error is negligible and that it remained always smaller than the error range of our measurements (±5%). All calculations were performed by considering ideal gas law. Besides, we also note that any possibility of H_2 lost by its dissolution in water was also neglected. The hydrolysis reaction of $NaBH_4$ is contained in the basic solution. This basic medium has a key

role both in increasing the shelf life of H_2 and suppressing the self-hydrolysis of $NaBH_4$, as a stabilizer [35,36]. Furthermore, with the inclusion of released OH^- ions in the hydrolysis of $NaBH_4$, this can increase appropriate rate of hydrogen production at a certain concentration value [37]. The flask was placed on a hot plate magnetic stirrer and the outlet pipe coming out of the flask was placed inside a water-filled burette, which was placed in a beaker filled with water to capture the evolved H_2 inside of the burette (Figure 1). 20 mg of catalyst was placed in the flask and the $NaBH_4$ solution was added to the flask, thereafter the flask was sealed immediately. As all catalysts required a short induction period, it was ensured that no H_2 was lost to the environment. As seen from Figure 1, hydrogen production was performed in the flask with a thermometer to control the reaction temperature. The reaction of hydrolysis of $NaBH_4$ is given in Equation 1 [1].

$$NaBH_4 + 2H_2O \rightarrow NaBO_2 + 4H_{2(g)} \quad (1)$$

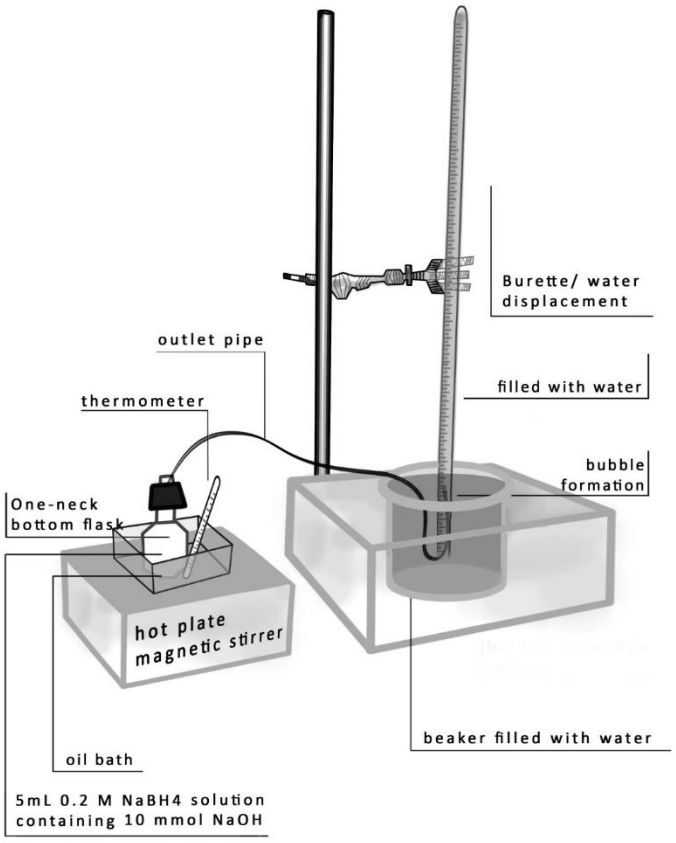


Figure 1. Experimental setup for hydrogen generation from the hydrolysis of $NaBH_4$.

For all catalyst particles, the hydrolysis reaction in was carried out at 25 °C. The specific hydrogen production rate (ml H_2 min^{-1} g_{cat}^{-1}) was calculated according to the linear portion of the volume of produced H_2 versus reaction time plots [38]. Hydrolysis at different temperatures (30, 35, 40, and 45 °C) was also conducted and catalytic performance with increasing temperature was examined for the best performing sample. The Arrhenius plot was obtained and activation energy was calculated for this catalyst. Furthermore, the durability of the best-performing catalyst (S4@850) was measured as described elsewhere [39]. Recyclability tests were performed at room temperature where first a standard experiment was performed using 20 mg of catalyst with a 5 mL 0.2 M $NaBH_4$ solution containing 10 mmol NaOH. After the $NaBH_4$ in the solution was hydrolyzed completely, the same amount of $NaBH_4$ was added to test the durability of the catalyst. The addition of the same amount of $NaBH_4$ was continued until the

same catalytic performance was measured (5th cycle). To indicate and summarize the research methodology, a flowchart of the process used in the study is shown in Figure 2.

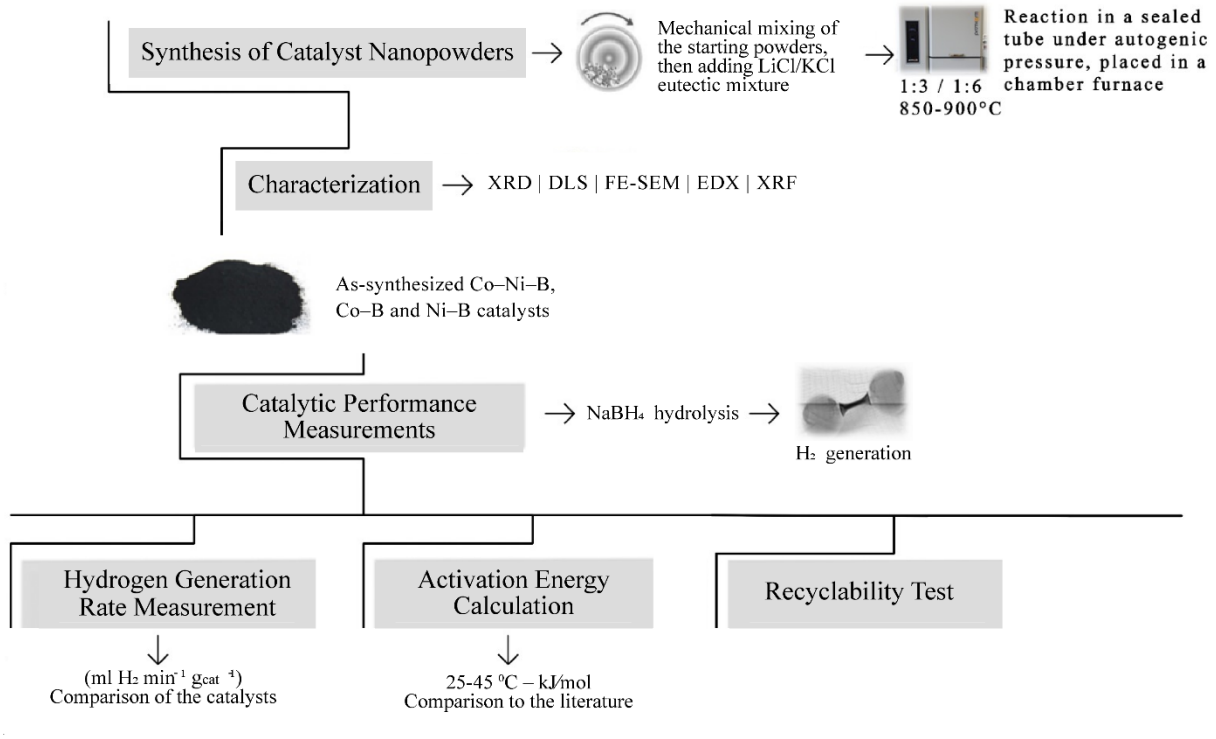


Figure 2. Flowchart of the process used in the study.

3. Results and Discussion

3.1. Phase and chemical analyses of the synthesized catalysts

Figures 3 and 4 show the XRD patterns of the synthesized Co–Ni–B catalysts. The XRD patterns of the synthesized Co–B and Ni–B binary boride catalysts are presented in Figure S2, (in SI). As seen from the XRD analyses, all the powders synthesized at 850 and 900°C by using $CoCl_2$–$NiCl_2$–$NaBH_4$ mixtures consist of crystalline Co/Ni–B and Co–Ni–B-based metal boride composites. The used synthesis method enabled the simultaneous formation of the binary/ternary compounds via a one-step reaction of $CoCl_2$–$NiCl_2$–$NaBH_4$ mixture in an inorganic molten salt environment. According to the changing synthesis parameters, different compositions of the metal boride composites were formed including the crystalline CoB, Co_2B, Co_5B_{16}, NiB, Ni_4B_3, and $Ni_2Co_{0.67}B_{0.33}$ phases. Table S1 presents the ICDD Card information

for all the crystalline phases, while Table S2 shows the indices for the corresponding diffraction peaks of the all obtained phases (in SI). It is clear that the ratio of metal chlorides to $NaBH_4$ and reaction temperature significantly affected the formed phases, which made the preparation of different catalysts possible. As the $CoCl_2$–$NaBH_4$ or $NiCl_2$–$NaBH_4$ binary systems were used as starting mixtures with a ratio of metal chlorides to $NaBH_4$ as 1:6, single phases of CoB or Ni_4B_3 binary borides were formed, respectively (Figure S2). However, as the $CoCl_2$–$NiCl_2$–$NaBH_4$ ternary system was used with a ratio of metal chlorides to $NaBH_4$ as 1:3 and 1:6, mixed compositions containing different binary and ternary compounds were achieved (Figures 3 and 4). The formation of $Ni_2Co_{0.67}B_{0.33}$ ternary phase was only observed in the S2@850 sample (Figure 3(c)), where elemental boron was added to the starting mixture (+2 mole of B). On the other hand, nickel-rich Ni_4B_3 phase was occurred, when the starting ratio was 1:6 (Figure 4), whereas the formed phase including Ni was NiB in the case of the ratio as 1:3 (Figure 3). Thus, playing with the metal chloride to $NaBH_4$ ratio seems to affect the phase of the Ni-containing crystal. On the other hand, despite the use of the same reaction temperature and starting ratio (Figure 4(a) and (c)), mechanical alloying of the starting mixture prevented the formation of NiB and thereby resulted in the powders containing only CoB and Ni_4B_3 phases. In overall, it can be indicated from the XRD peaks that the increase in reaction temperature from 850 to 900 °C caused a slight increase in the crystallinity of the CoB phase (Figures 3(b) and 4(b)).

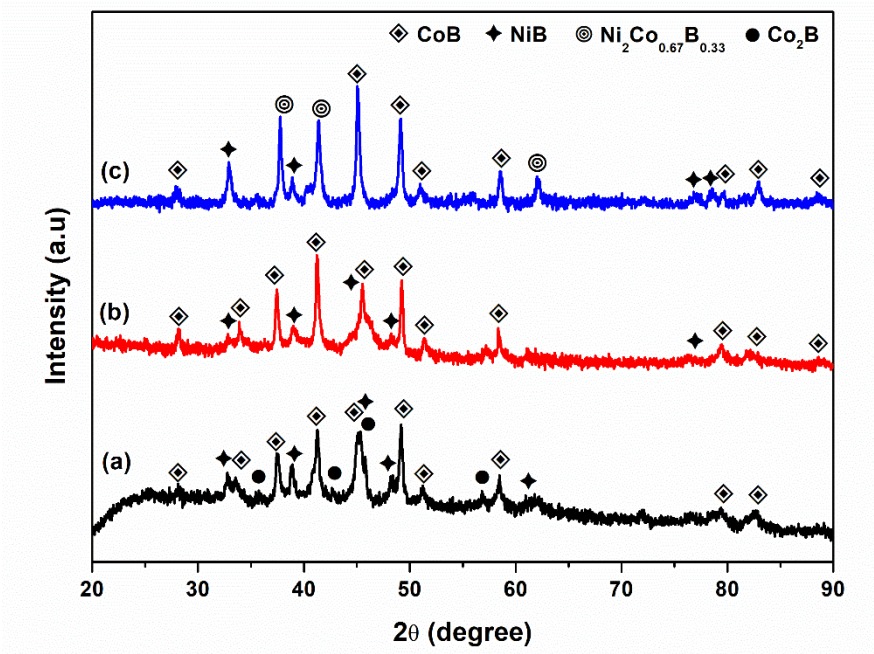


Figure 3. XRD patterns of the synthesized Co–Ni–B catalysts: (a) S1@850, (b) S1@900 and (c) S2@850.

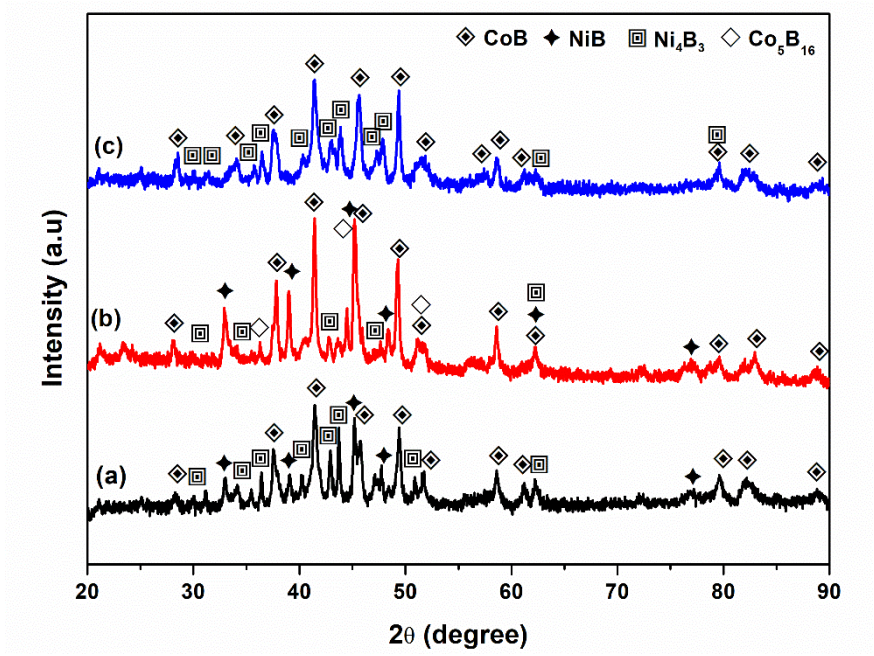


Figure 4. XRD patterns of the synthesized Co–Ni–B catalysts: (a) S3@850, (b) S3@900 and (c) S4@850.

Table 2 summarizes the phase compositions obtained from the XRD patterns and presents the chemical analyses of the synthesized catalysts. Chemical analyses of the ternary systems revealed the Co and Ni elemental compositions as similar values for all compositions in

between 31–41 and 32–45 wt. %, respectively (Table 2). Only the S3@900 sample with high boron content showed an exception with the Co and Ni values at about 28 wt. %, most likely due to the high amount of starting $NaBH_4$ and relatively high reaction temperature of 900°C. On the other hand, the powders contain slight amount of K and Cl impurities (0.2–0.9 wt. %) stemming from the KCl inorganic compound, which could not be completely removed from the system. It could be declared that this Cl impurity may have a decreasing effect on the hydrogen generation rate. Thus, this impurity are trace amounts and almost in the same range for all of the catalysts.

Table 2. Phase composition of the synthesized catalysts.

Sample Name	Phase and chemical analysis				
	Formed crystalline phases (XRD analysis)	**Elemental composition (wt. %) (XRF analysis)**			
		Co	**Ni**	**K**	**Cl**
S1@850	CoB–NiB–Co_2B	40.3	41.6	0.6	0.9
S1@900	CoB–NiB	31.8	32.5	-	0.4
S2@850	CoB–NiB–$Ni_2Co_{0.67}B_{0.33}$	40.7	44.7	-	0.2
S3@850	CoB–Ni_4B_3–NiB	40.5	38.5	0.9	-
S3@900	CoB–Ni_4B_3–NiB–Co_5B_{16}	28.6	28.9	0.3	0.9
S4@850	CoB–Ni_4B_3	35.0	36.2	0.5	0.6
S5@850	CoB	82.8	-	0.4	0.2
S6@850	Ni_4B_3	-	85.4	0.5	-
CP	Co_2B–Co_3B				

3.2. Microstructures and particle sizes of the synthesized catalysts

Figure 5 presents the FE-SEM images of the synthesized Co–Ni–B, Co–B and Ni–B catalysts. It is observed that the particles possess a spherical-like morphology, which can be attributed to the autogenic pressure present inside of the sealed tubes during the synthesis process. The spherical-like morphology of the catalysts can be better observed in the high magnification FE-SEM images of the selected powders (Figure S3, in SI). SEM images of the particles present a homogeneous distribution throughout the samples, most likely because of the effect of roll milling or mechanical alloying processes during the preparation step, and also the molten salt environment of the synthesis process. Especially the S4@850 sample revealed a uniform and

fine microstructure due to the positive effect of mechanical alloying. To better observe its whole microstructure, the low-magnification SEM image of this sample is presented in Figure S4 (in SI). Nano-sized particles are seen in agglomerated forms in low magnification image of S4@850 sample (Figure 5(d)). In compliance with the SEM images, all XRD patterns exhibited peak broadening indicating the nanocrystalline character of the obtained particles (Figures 3 and 4).

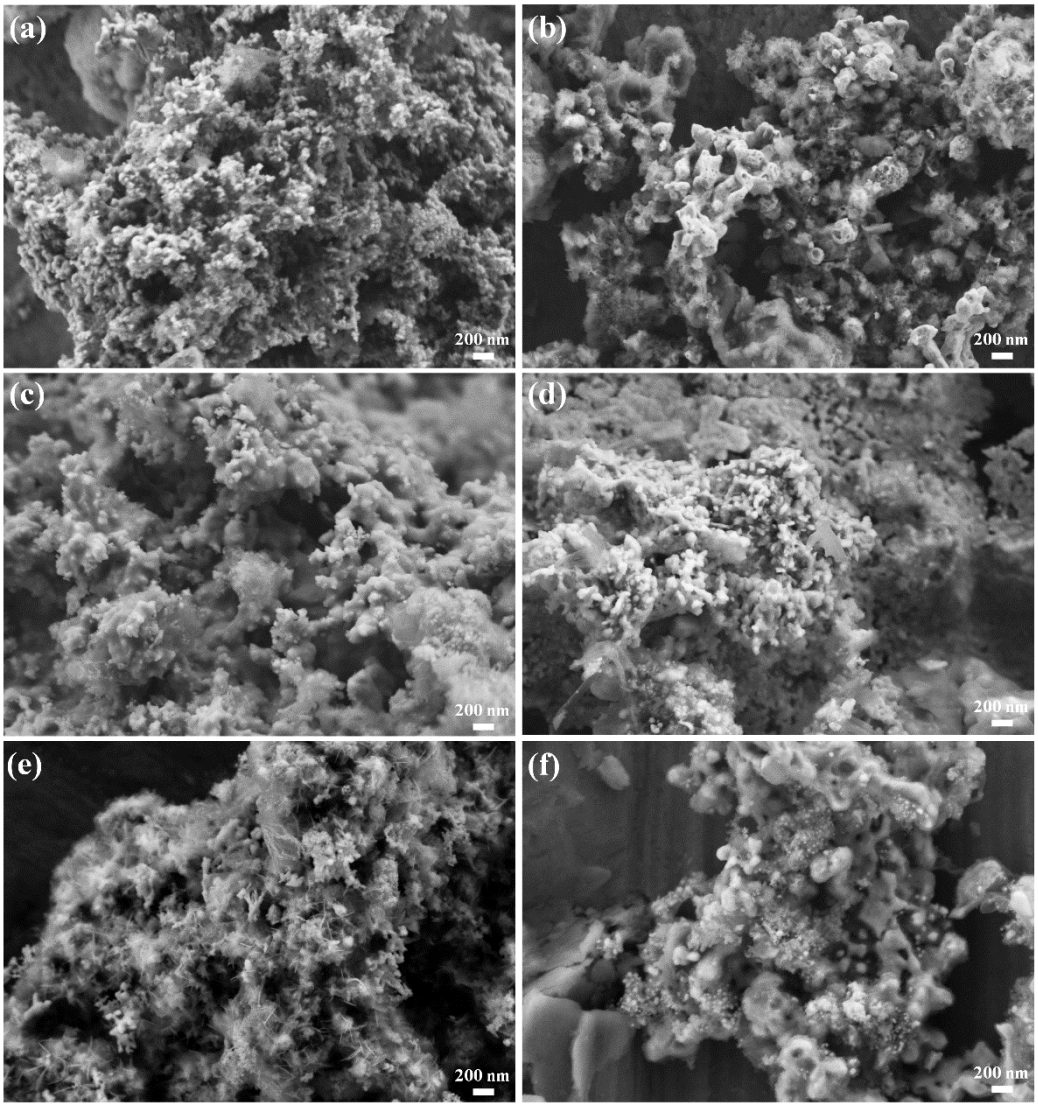


Figure 5. Secondary electron FE-SEM images of the synthesized Co–Ni–B, Co–B and Ni–B catalysts: (a) S1@850, (b) S1@900, (c) S3@900, (d) S4@850, (e) S5@850, and (f) S6@850.

In order to confirm the uniformity of all elements distribution, SEM/EDX analyses are performed on the catalysts. The homogenous distribution of nickel, cobalt and boron elements can be observed in Figure 6, for the selected sample of S4@850. The elemental Co and Ni maps coincide entirely with the elemental B map, supporting the simultaneous presence of cobalt and nickel boride phases detected by XRD analysis (Figure 4c). EDX analyses for the other catalysts are given in Figure S5 (in SI) to show the distribution of all elements throughout the samples. The weak signals of B particles in all analysis results can be associated with the suppression effect of the other strong signals of the Co and Ni elements. Furthermore, any signals of other elements were not detected during the EDX analyses, which also proves the purity of the catalyst powders.

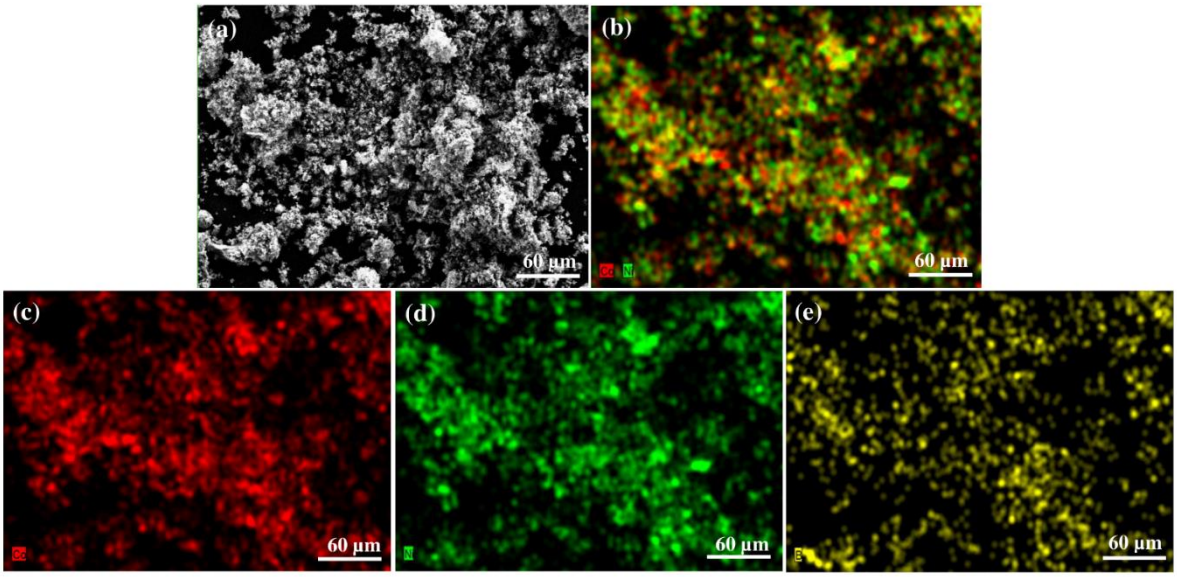


Figure 6. (a) SEM image of sample S4@850, (b) EDX mapping of sample S4@850, (c) EDX mapping of Co, (d) Ni, (e) B in sample S4@850.

Figure 7 shows the particle size measurements of the catalysts that is derived from the SEM and DLS analyses. As seen in Figure 7a, average particle sizes of the powders are changing from ~51 to 94 nm. Particle size distribution graphs of the selected samples are shown as representative for all samples, which have a uniform particle size distribution (Figure 7b and

7c). The average particle size of S4@850 sample is determined as 62.4 and 65 nm according to the SEM and DLS analyses, respectively, in which comparable values are obtained despite of the different techniques. The data also indicate that when using the same ratio of metal chlorides to $NaBH_4$ during the synthesis, an increase in the reaction temperature from 850 to 900 °C resulted in an increase in the particle size. Namely, while the particle size in S1@850 was 51.7 nm, the particle size in S1@900 was 94.0 nm. Similarly, the particle size increased from 68.2 nm to 77.8 nm when using a higher reaction temperature for the samples obtained by using a ratio of metal chlorides to $NaBH_4$ as 1:6 (S3@850 and S3@900). On the other hand, some measured average particle sizes of the powders synthesized at the same temperature showed no obvious change, like in the samples S3@850 (68.2 nm) and S4@850 (62.4 nm). This is seen convenient for a comparison of the catalytic performances of the metal boride composites to see the sole effect of different phases on the hydrogen production. Finally, the analysis results showed that the as-prepared catalysts are in high-purity and consisting of nano-size particles with similar morphology and uniform distribution.

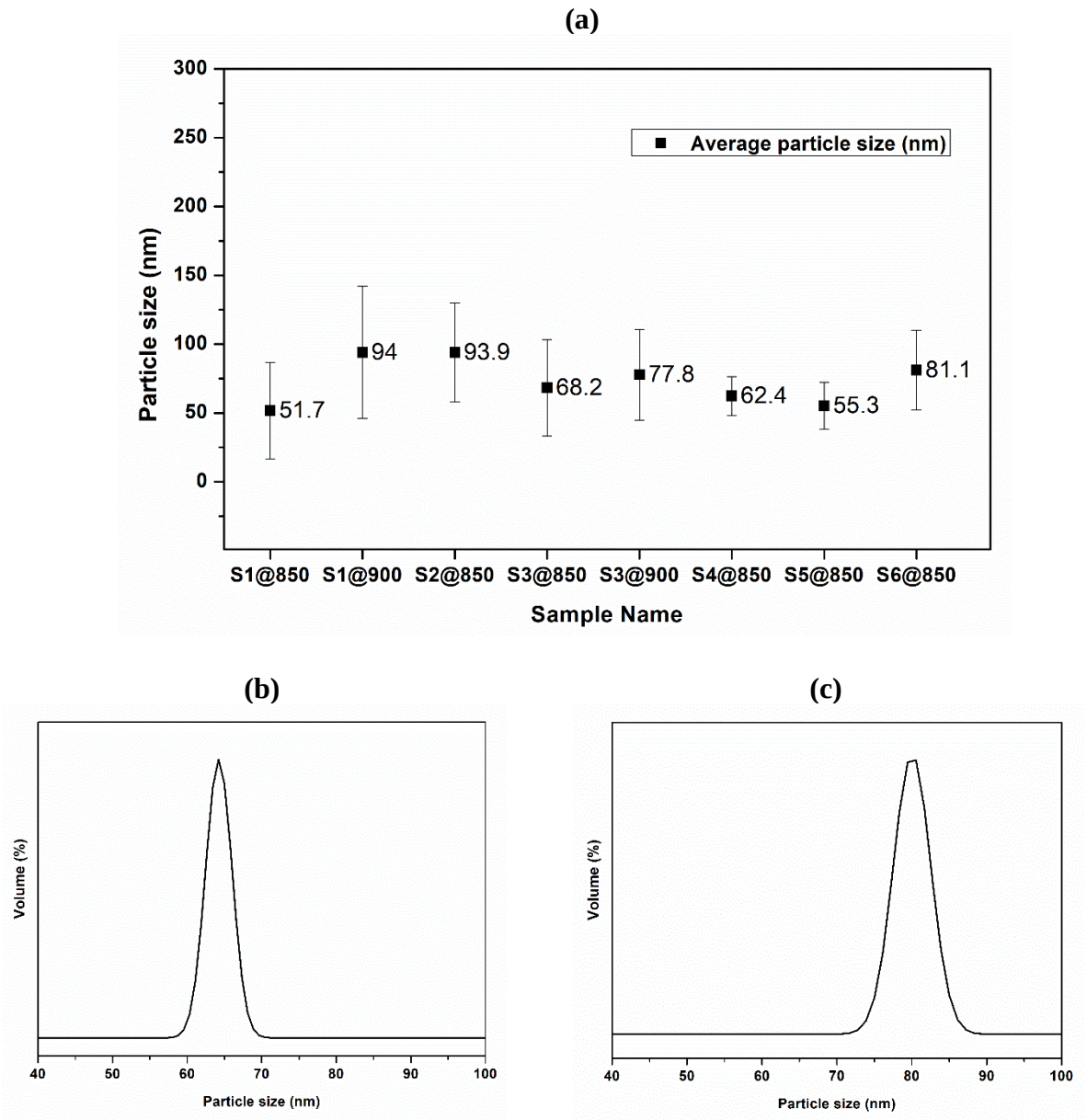


Figure 7. (a) Average particle size comparison of all Co–Ni–B, Co–B and Ni–B catalysts, derived from FE-SEM analysis (error bars indicate the standard deviation of twenty measurements) and representative size distribution graphs of (b) S4@850 and (c) S6@850 derived from DLS particle size analysis.

3.3. Catalytic performance measurements

Figure 8 shows the evolution of equivalent hydrogen per mole of $NaBH_4$ versus time plot for the hydrolysis of $NaBH_4$ solution in the presence of different Co–Ni–B catalysts at 25°C (The evolution of hydrogen (mL) versus time plot for each experiment can be seen in Figure S6).

For all catalysts, the amount of hydrogen produced is almost directly proportional to the reaction time, which indicates the stable catalytic activity of the catalysts. The data in Figure 8 show that the S4@850 catalyst with CoB–Ni_4B_3 phases showed the highest catalytic activity. Among the as-prepared catalysts, the powder containing the single Ni_4B_3 phase (S6@850) showed no catalytic activity and therefore, it is not included in the graph in Figure 8. Such was the case for the commercial cobalt boride powder (CP), which had no catalytic activity as well. Furthermore, it is seen that the S5@850 catalyst containing the single CoB phase showed lower catalytic activity compared to the other catalysts. It is interesting to note that as these catalysts including the Ni_4B_3 phase or CP showed no catalytic activity alone, the powders with different boride phases together or with ternary boride compound including the CoB-Ni_4B_3 and $Ni_2Co_{0.67}B_{0.33}$ showed very high activities. Thus, synergetic effect of the CoB and Ni_4B_3 crystalline phases in Co–Ni–B based catalyst is able to significantly increase the catalytic activity and decrease the reaction time, as compared to those obtained with CoB or Ni_4B_3 phases alone. Similar findings were reported for the amorphous phases, where the Co–Ni–B system provided higher activity compared to CoB or NiB alone for hydrogen production by $NaBH_4$[17,19,40]. In another study, Raney catalysts obtained by the alloying of Raney Ni and Raney Co provided enhanced performance for $NaBH_4$ hydrolysis compared to only Ni or Co [11]. Comparing all the catalysts investigated in this study, S4@850 and S3@850 catalysts containing the CoB–Ni_4B_3 and CoB–Ni_4B_3–NiB phases, respectively, demonstrated the highest catalytic performance under the same conditions at 25°C.

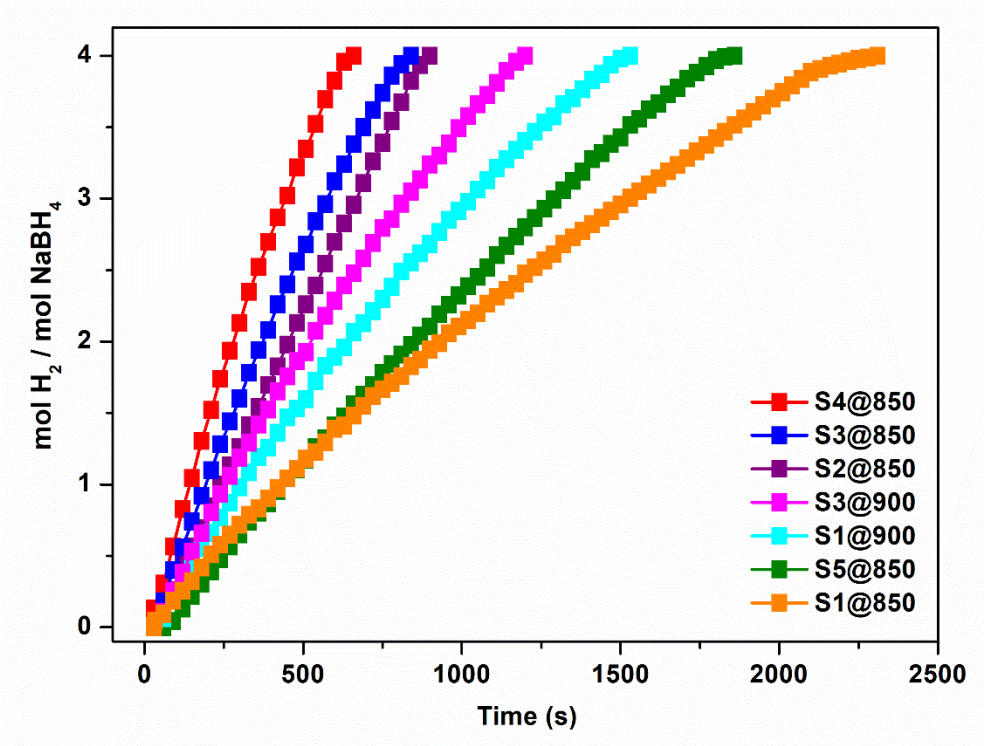


Figure 8. The evolution of equivalent hydrogen per mole of $NaBH_4$ versus time plot for the hydrolysis of 5 mL of 0.2 M $NaBH_4$ containing 10 mmol NaOH in the presence of different catalysts (20 mg) at 25 °C.

Figure 9 shows the effect of binary and composite boride catalysts on the hydrogen generation rate from $NaBH_4$ solution. To obtain the data presented in Figure 9, hydrogen production rates were calculated based on the graphs of hydrogen production volume versus time (min) and the unit of catalyst amount (g); and so the hydrogen production rate was reported in ml H_2 min^{-1} g_{cat}^{-1}. It is known that the alkaline $NaBH_4$ solution is highly stable at high pH values [21]. In recent experimental studies, it has been determined that with the use of a suitable catalyst, hydrogen can be produced from sodium borohydride even in environments with a pH value greater than 11 [41]. As can be clearly seen from the comparison of values in Figure 9, the catalysts containing the CoB–Ni_4B_3 and CoB–Ni_4B_3–NiB phases that were used during the hydrolysis of $NaBH_4$ had provided an important catalytic activity advantage in the rate of hydrogen production (500.0 and 404.6 ml H_2 min^{-1} g_{cat}^{-1}, respectively) compared to all other powders. According to Figures 8 and 9, one can see that the catalysts containing the Ni_4B_3 phase

(S4@850 and S3@850) provides enhanced hydrogen production rates compared to the NiB containing samples (S1@850, S1@900, S2@850). S3@900, containing the dominant NiB phase with slight amount of Ni_4B_3 (Figure 4(b)), provided lower catalytic performance compared to the catalysts containing only Ni_4B_3, as well (Figure 9). The presence of Ni plays an important role as it is proposed by Guo and coworkers [42]. The presence of well-dispersed Ni sites with an optimal content was found to prompt hydrogen spillover from the surface thereby hindering H_2 agglomeration and coverage on the active Co sites [42]. Based on our findings the Ni-rich phase, Ni_4B_3, act as a better promoter than NiB. Thus, using a mole ratio of metal chlorides to $NaBH_4$ of 1:6 during the synthesis seems more desirable (Table 2). When comparing the best performing catalysts containing the Ni_4B_3 phase (S4@850 and S3@850), the existence of NiB phase in the S3@850 sample seem to reduce the catalytic performance. Because the average particle sizes (68.2 and 62.4 nm) and purities of these catalysts (impurities ≤0.9 and 1.1 wt. %) are comparable to each other (Figure 7a and Table 2), the type of formed crystalline phases are the main influential fact of the H_2 generation rates. Slightly lower particle size of S4@850 (62.4 nm) than S3@850 (68.2 nm) might also contribute to the enhancement of the catalytic performance. On the other hand, S1@850 which has the Co_2B phase provided the lowest activity. The presence of Co_2B phase in the structure of the catalyst might decrease chemical stability of the composite borides because of low stability of the metal-rich boride compound of Co–B system. Given the higher hydrogen production rate of 246.4 ml H_2 min^{-1} g_{cat}^{-1} of the S1@900 sample containing the CoB–NiB phases supports this claim, even though this sample has a twice higher particle size compared to S1@850 (Figure 7a). It is worth to mention here that the CP catalyst containing the Co_2B–Co_3B phases did not present a catalytic activity. This indicates that the metal rich cobalt boride compounds with low chemical stability are not efficient to be used as catalysts in the present system.

Figure 9 clearly demonstrates also the difference between the composite and binary metal boride catalysts, where binary boride catalysts give either very low rate or do not give an activity. It is widely known that the regular Co–B systems provide low surface area, poor thermal stability and broadly distributed particle size [40]. Fernandes and coworkers determined that mixed Co–Ni together with B atoms performs much better as the electron density over the metals are enriched by the electron transfer from B. It was found that the Co and Ni metals exchange electrons much easier in the Co–Ni–B system, compared to the Co–B and Ni–B catalysts [17]. It was also reported that the mole ratio of Co/(Co+Ni) in the amorphous catalyst powders highly affected the hydrogen production rates [17]. In our findings however, the alterations in catalytic performances can be directly related to the existing crystalline phases in the catalyst structures, since the Co/(Co+Ni) mole ratios are the same as 0.5 for all catalysts (Table 2). Furthermore, the addition of Ni to Co–B catalyst was found to enhance the stability of the final catalyst [43]. In addition to the obtained phases, the nanocrystalline character of the as-prepared catalysts (Figures 3-7) has also a positive effect on the achieved hydrogen production rates. It is a known method to reduce sizes of the particles used as catalyst in order to accelerate the hydrolysis of $NaBH_4$ due to the higher surface area thereby increasing the number of active sites [42]. Based on the obtained results in this study, the authors validate the claim that catalysts with a fine and uniform particle size, exhibit increased hydrogen generation rates [44]. The inorganic molten salt technique as a low-cost and simple synthesis method in this study makes it possible for the preparation of the nanocrystalline catalysts.

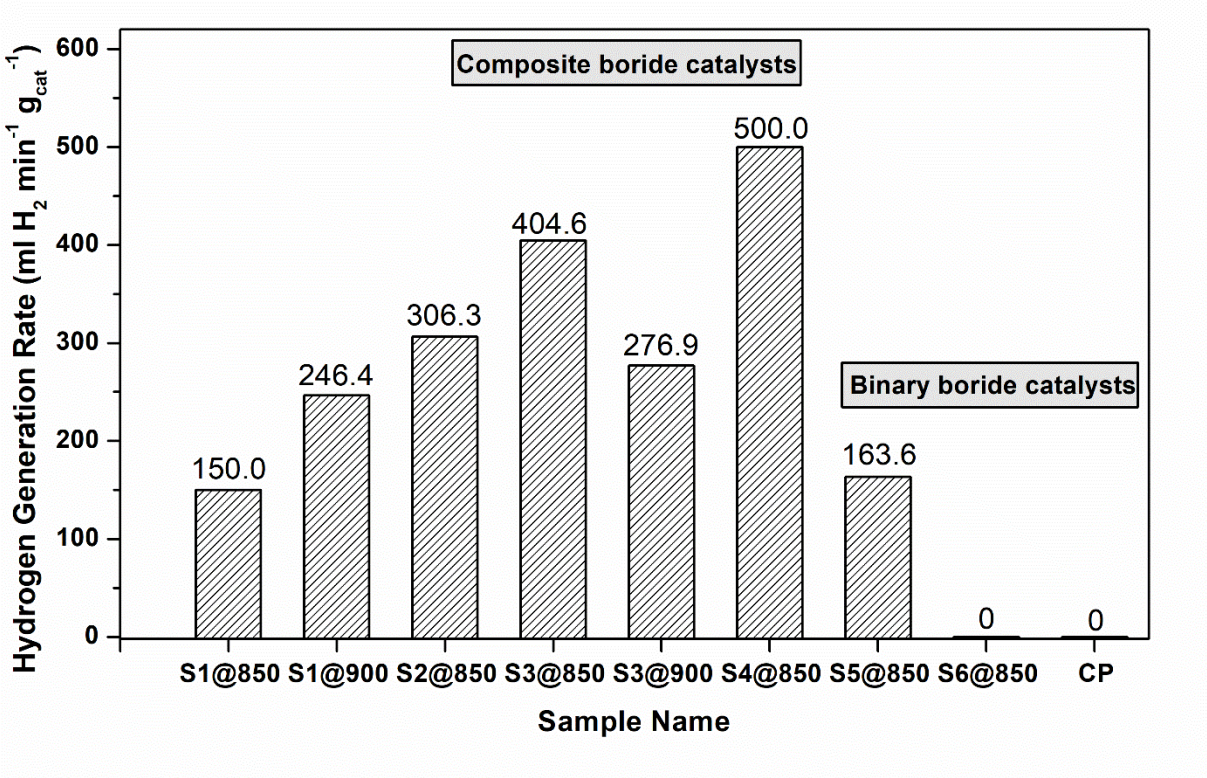


Figure 9. Effect of binary and composite boride catalysts on the hydrogen generation rate from $NaBH_4$ solution. (Hydrolysis conditions: 5 mL of 0.2 M $NaBH_4$ containing 10 mmol NaOH in the presence of different Co–Ni–B, Co–B and Ni–B catalysts (20 mg) at 25 °C).

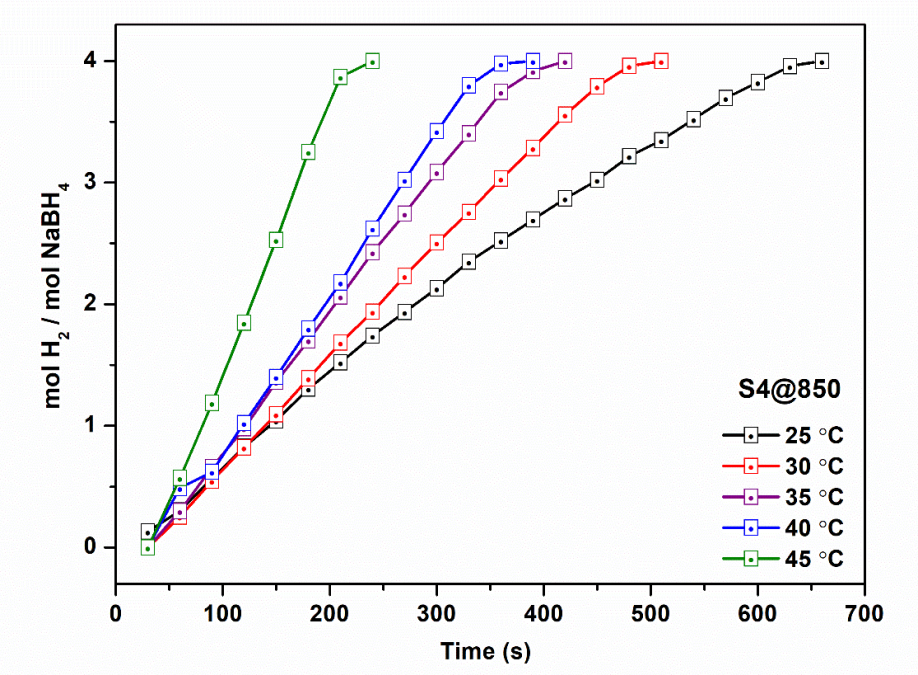
In order to determine the effect of different temperatures on catalytic performance, catalytic hydrolysis of 0.2 M sodium borohydride ($NaBH_4$) was analyzed in the presence of 20 mg S4@850 catalyst at various temperatures (25, 30, 35, 40, and 45°C). Figure 10a shows the evolution of equivalent hydrogen per mole of $NaBH_4$ versus time plot in the presence of S4@850 catalyst. As seen from Figure 10a, the rate of hydrogen production increased as expected with the increase in temperature. The hydrogen production rates obtained at various temperatures are given in Table 3 in ml H_2 min^{-1} g_{cat}^{-1} and it is seen that the hydrogen production rate at 45°C has reached 1257.1 ml H_2 min^{-1} g_{cat}^{-1}. The Arrhenius curve for the activation energy calculation has been extracted and the Arrhenius curve of the hydrogen production rate between 25-45°C is presented in Figure 10b. In the activation energy calculation, the data points closer

to the differential conversion region were used. The activation energy (E_a) of $NaBH_4$ hydrolysis reaction can be obtained from the Arrhenius equation given in Eq.(2) [45].

$$\ln(k) = \ln(A) - \frac{E_a}{RT} \qquad (2)$$

Where k is the rate constant of the reaction, A is pre-exponential factor, E_a is the apparent activation energy (kJ/mol), R is molar gas constant (8.314 J/K/mol) and T is the reaction temperature (K). We want to note that the rate of the hydrogen generation was determined as zero-order for S4@850 as shown in Figure S7, comparing data in the zero-, first-, and second-order reaction kinetic models. According to Figure S7a, data shows that the hydrolysis obeyed zero-order kinetics as the concentration of $NaBH_4$ shows a linear relation with reaction time at a reaction temperature of 25°C. Consistently, several other investigations reported the reaction kinetics of $NaBH_4$ as zero-order [13,21,46,47]. The activation energy for $NaBH_4$ hydrolysis as catalyzed by S4@850 sample was calculated as 32.7 kJ/mol from the slope of the graph in Figure 10b, which has been created using the zero-order rate constants provided in Table S3. Rate constant were determined using the slope of the zero-order reaction kinetic models at 25, 30, 35, 40, 45 °C (Figure S7a, Figure S8).

(a)



(b)

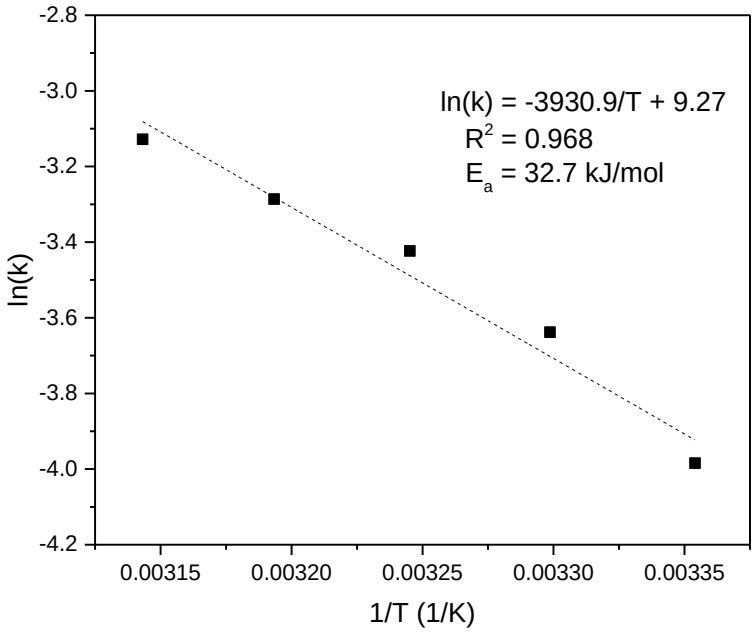


Figure 10. The evolution of equivalent hydrogen per mole of $NaBH_4$ versus time plot in the presence of S4@850 catalyst: (a) at different temperatures and (b) the corresponding Arrhenius plot (Hydrolysis conditions: 5 mL of 0.2 M $NaBH_4$ containing 10 mmol NaOH in the presence of 20 mg of the catalyst).

Table 3. Hydrogen generation rates at five different temperatures by hydrolysis of $NaBH_4$ solution in the presence of S4@850 catalyst and calculated activation energy value. (Hydrolysis conditions: 5 mL of 0.2 M $NaBH_4$ containing 10 mmol NaOH in the presence of 20 mg of the catalyst)

Catalyst Powder	**Hydrolysis exp. temperature (°C)**	**Hydrogen generation rate (ml H_2 min^{-1} g_{cat}^{-1})**	**Activation energy (kJ/mol)**
S4@850 ($CoB–Ni_4B_3$)	25	500.0	32.7
	30	600.0	
	35	733.3	
	40	777.3	
	45	1257.1	

Table 4 displays the hydrogen generation rates and calculated activation energy values for the hydrolysis of $NaBH_4$, as catalyzed by various reported catalysts. It is well known that the NaOH and $NaBH_4$ concentrations considerably affect the hydrolysis rates [9,42,45,47,48]. Since sodium borohydride is used here as a source of hydrogen, the increase in the amount of hydrogen with the increase wt. % of $NaBH_4$ is an expected result. Moreover, optimizing the basicity of the hydrolysis solution also promotes hydrogen generation. The Cl impurities remaining in the catalyst (Table 2) material also have an effect of reducing the hydrogen generation rate. On the other hand, the obtained activation energy value of the $NaBH_4$ hydrolysis reaction as catalyzed by S4@850 sample (32.7 kJ/mol) is obviously lower than that of previously reported catalysts, whose activation values were reported as 57.8, 72.5, 45, 42.8 kJ/mol [8,9,18,49]. As seen from Table 4, only carbon-supported boride catalyst showed a very low activation energy value (23.5 kJ/mol), because of its well-dispersed characteristics having more active sites (due to the CNTs promoters) and hence accelerating the hydrolysis [3]. In addition, there are also samples with 29.3 and 26.8 kJ/mol activation energy values; however, when the synthesis methods are examined, it can be seen that there are tetrahydrofuran (THF) organic compound additions as well as raw materials [4,51]. The activation energy value obtained in the present study is a remarkable value (32.7 kJ/mol) among those reported in the literature, since no supporting or coating material was used here. This result may be related to the fine distribution and homogeneous microstructure of the S4@850 sample (Figures 5 and 7), the Ni-rich phase Ni_4B_3 and the absence of Co_2B, thanks to the synthesis method used in this study. Further effect of the surface properties and coating conditions of the composite boride catalysts on the hydrogen generation would be interesting to study in the future. It is interesting to note that the studies on the performances of Co–Ni–B or Co–B catalysts for $NaBH_4$ hydrolysis is very limited (as listed in Table 4) and all the catalysts powders are in amorphous phase, except for the reports by Wei et al [49], and our study. Thus, it is thought that the

achievement of activation energy value lower than those of Co–Ni–B based powders that are reported in the literature is related to the presence of non-amorphous, nanocrystalline and highly chemically stable metal boride compounds in the structure of the synthesized catalyst [12]. As suggested by Gupta et al., even though it is widely accepted that completely crystalline phases of metal boride are less active than their amorphous counterparts for the electrochemical water splitting, tailoring the crystalline metal borides so that more active sites are exposed to the reactants can be promising [50]. Here we showed that, the crystalline metal borides provide favorable performance with amorphous counterparts for $NaBH_4$ hydrolysis (Table 4), thereby creating new opportunities for the utilization of these nanocrystalline metal borides.

Table 4. Comparison of hydrogen generation rates (for the hydrolysis of $NaBH_4$ at 25 °C) and activation energy between the as-prepared catalyst and other catalysts at 25°C that are reported in the literature.

Catalyst Powder	**Hydrolysis Conditions**	**Hydrogen generation rate (ml H_2 min^{-1} g_{cat}^{-1})**	**Activation energy (kJ/mol)**	**References**
Co–B	0.75 wt.% $NaBH_4$ 8 wt.% NaOH	1127	57.8	[7]
Co–B	0.01 wt.% $NaBH_4$ 0.01 wt.% NaOH	681	45.0	[17]
Ni–B	0.01 wt.% $NaBH_4$ 0.01 wt.% NaOH	100	-	[17]
Co(0.85) –Ni–B	0.01 wt.% $NaBH_4$ 0.01 wt.% NaOH	1175	34.0	[17]
Co–B–O	5 wt.% $NaBH_4$ 2 wt.% NaOH	7450	26.8	[51]
Ni–B	0.5 wt.% $NaBH_4$ 1 wt.% NaOH	146	-	[8]
NiB/$NiFe_2O_4$	0.5 wt.% $NaBH_4$ 1 wt.% NaOH	299	72.5	[8]
Co–B–O@Co_2B	1 wt.% $NaBH_4$ 5 wt.% NaOH	3850	29.3	[4]
Co-Ni-B	2.7 wt.% $NaBH_4$ 15 wt.% NaOH	2608	62.0	[21]
Co–Ni–B/Cu sheet	5 wt.% $NaBH_4$ 1 wt.% NaOH	14778	42.8	[49]
Co–B–10CNT	5 wt.% $NaBH_4$ 5 wt.% NaOH	12000	23.5	[3]
CoB–Ni_4B_3 (S4@850)	0.75 wt.% $NaBH_4$ 8 wt.% NaOH	500	32.7	present study

Recyclability tests were performed for the best performing catalyst (S4@850) to ensure that S4@850 maintains its catalytic performance after various cycles. A standard experiment was performed as the first cycle at room temperature. After assuring the hydrolysis of $NaBH_4$ completely, the same amount of $NaBH_4$ was added at each cycle to remeasure the activity of the catalyst powder at identical conditions. Figure 11 shows that the performance of S4@850 relatively decreases; however, the catalytic activity is retained even after multiple cycles. Furthermore, the performance does not change after the 4^{th} cycle as illustrated in Figure 11.

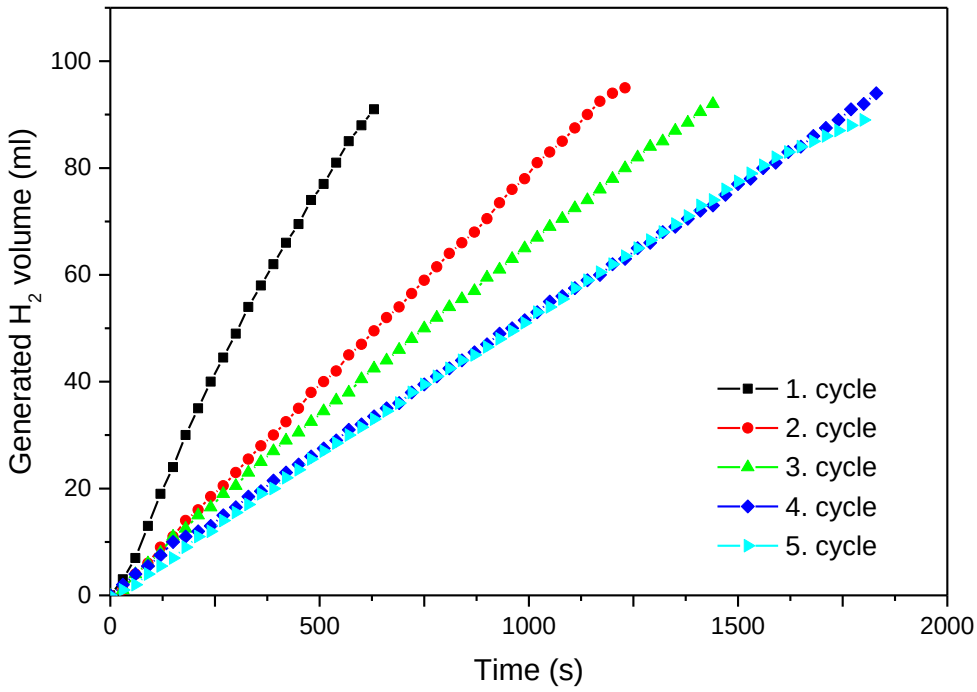


Figure 11. Evolution of hydrogen (mL) versus time plot for S4@850 showing the recyclability of the catalyst for 5 cycles. (Hydrolysis conditions for each cycle: 5 mL of 0.2 M $NaBH_4$ containing 10 mmol NaOH in the presence of 20 mg of the catalyst).

Consequently, Co–Ni–B based nanocrystalline powders as synthesized within the scope of this study are materials that are very suitable for use as catalysts of low activation energy in $NaBH_4$ hydrolysis. It has been concluded that the nickel-rich crystalline Ni_4B_3 binary metal boride phase that was synthesized as cobalt-nickel-boron based composite powders significantly increase catalytic performance of the $NaBH_4$ hydrolysis for hydrogen production.

4. Conclusion

Innovative metal boride composite catalysts having different compositions (including the crystalline CoB, Co_2B, Co_5B_{16}, NiB, Ni_4B_3, and $Ni_2Co_{0.67}B_{0.33}$ phases) were synthesized via a one-step direct reaction of $CoCl_2$–$NiCl_2$–$NaBH_4$ in an inorganic molten salt environment. The obtained compositions were varied by changing the mole ratio of metal chlorides to sodium borohydride as 1:3/1:6 and the reaction temperature as 850/950°C. The reactions for binary systems of $CoCl_2$–$NaBH_4$ and $NiCl_2$–$NaBH_4$ respectively resulted in pure crystalline CoB and Ni_4B_3 formation, whereas the reactions in $CoCl_2$–$NiCl_2$–$NaBH_4$ ternary system resulted in mixed compositions containing different binary and ternary compounds. Analyses of the powders illustrated that all the as-prepared catalysts are in high-purity with average particle sizes ranging in ~51 to 94 nm and consisting of nanocrystalline phases. Catalytic performance tests showed that the existence of nickel rich Ni_4B_3 crystalline phase in the composite catalyst and the synergetic effect of the different cobalt and nickel boride phases had a positive role on the enhancement of catalytic activities. The composite catalyst containing the CoB–Ni_4B_3 phases exhibited the highest H_2 production rate (500.0 $ml.min^{-1}.g^{-1}$), whereas the Co–B and Ni–B based catalysts containing the crystalline phases of unstable cobalt borides or single Ni_4B_3 did not show any catalytic activity. The activation energy of the best performing catalyst (CoB–Ni_4B_3) was calculated as 32.7 kJ/mol, which is remarkably lower than those of many other Co–Ni–B based catalysts reported in the literature. Recyclability tests were also executed on the best performing catalyst. In these tests carried out under room temperature, it was observed that the powder did not lose its catalytic activity despite multiple cycles. Even though the cycle number was increased, the stability of the catalyst was not impaired. In summary, it was shown that metal boride composites in nanocrystalline structure can be used as alternative and stable catalysts for efficient hydrogen production from the hydrolysis of sodium borohydride.

Acknowledgments

This study was supported by “The Scientific and Technological Research Council of Turkey (**TÜBİTAK**)” with the project name "*Novel Low Temperature Synthesis of Cobalt–Metal–Boron (Metal=Ni, Fe, Ti) Based Ternary Metal Borides from Metal Chlorides: Characterization and Application Oriented Investigations on Catalyzer/Magnet/Hybrid Composite Fabrication*" and number of **117F178.** The authors would like to thank M.B. Yağcı for his help in SEM analysis. The authors A. Uzun and S.F. Kurtoğlu thank TARLA for collaborative research support.

REFERENCES

[1] Y. Kojima, K.I. Suzuki, K. Fukumoto, M. Sasaki, T. Yamamoto, Y. Kawai, H. Hayashi, Hydrogen generation using sodium borohydride solution and metal catalyst coated on metal oxide, Int. J. Hydrogen Energy. 27 (2002) 1029–1034. https://doi.org/10.1016/S0360-3199(02)00014-9.

[2] A. Züttel, P. Wenger, S. Rentsch, P. Sudan, P. Mauron, C. Emmenegger, LiBH4 a new hydrogen storage material, J. Power Sources. 118 (2003) 1–7. https://doi.org/10.1016/S0378-7753(03)00054-5.

[3] L. Shi, Z. Chen, Z. Jian, F. Guo, C. Gao, Carbon nanotubes-promoted Co–B catalysts for rapid hydrogen generation via NaBH4 hydrolysis, Int. J. Hydrogen Energy. 44 (2019) 19868–19877. https://doi.org/10.1016/j.ijhydene.2019.05.206.

[4] Y. Guo, R. Zhang, W. Hao, J. Zhang, Y. Yang, Multifunctional Co–B–O@CoxB catalysts for efficient hydrogen generation, Int. J. Hydrogen Energy. 45 (2020) 380–390. https://doi.org/10.1016/j.ijhydene.2019.09.008.

[5] N.P. Ghodke, S. Rayaprol, S. V. Bhoraskar, V.L. Mathe, Catalytic hydrolysis of sodium borohydride solution for hydrogen production using thermal plasma synthesized nickel nanoparticles, Int. J. Hydrogen Energy. 45 (2020) 16591–16605. https://doi.org/10.1016/j.ijhydene.2020.04.143.

[6] S.C. Amendola, S.L. Sharp-Goldman, M.S. Janjua, N.C. Spencer, M.T. Kelly, P.J. Petillo, M. Binder, A Safe, portable, hydrogen gas generator using aqueous borohydride solution and Ru catalyst, Int. J. Hydrogen Energy. 25 (2000) 969–975. https://doi.org/10.1016/S0360-3199(00)00021-5.

[7] J. Zhao, H. Ma, J. Chen, Improved hydrogen generation from alkaline NaBH4 solution using carbon-supported Co - B as catalysts, Int. J. Hydrogen Energy. 32 (2007) 4711–4716. https://doi.org/10.1016/j.ijhydene.2007.07.004.

[8] Z. Liang, Q. Li, F. Li, S. Zhao, X. Xia, Hydrogen generation from hydrolysis of NaBH4 based on high stable NiB/NiFe2O4 catalyst, Int. J. Hydrogen Energy. 42 (2017) 3971–3980. https://doi.org/10.1016/j.ijhydene.2016.10.115.

[9] G. Bozkurt, A. Özer, A.B. Yurtcan, Hydrogen generation from sodium borohydride with Ni and Co based catalysts supported on Co3O4, Int. J. Hydrogen Energy. 43 (2018) 22205–22214. https://doi.org/10.1016/j.ijhydene.2018.10.106.

[10] B.A. Yusuf, Y. Xu, N. Ullah, M. Xie, B-Doped carbon enclosed nickel nanoparticles: a robust, stable and efficient electrocatalyst for hydrogen evolution reaction, J. Electroanal. Chem. (2020). https://doi.org/10.1016/j.jelechem.2020.114085.

[11] B.H. Liu, Z.P. Li, S. Suda, Nickel- and cobalt-based catalysts for hydrogen generation by hydrolysis of borohydride, J. Alloys Compd. 415 (2006) 288–293. https://doi.org/10.1016/j.jallcom.2005.08.019.

[12] C. Wu, F. Wu, Y. Bai, B. Yi, H. Zhang, Cobalt boride catalysts for hydrogen generation from alkaline NaBH 4 solution, Mater. Lett. 59 (2005) 1748–1751. https://doi.org/10.1016/j.matlet.2005.01.058.

[13] D. Hua, Y. Hanxi, A. Xinping, C. Chuansin, Hydrogen production from catalytic hydrolysis of sodium borohydride solution using nickel boride catalyst, Int. J. Hydrogen Energy. 28 (2003) 1095–1100. https://doi.org/10.1016/S0360-

3199(02)00235-5.

[14] J. Li, F. Luo, Q. Zhao, L. Xiao, J. Yang, W. Liu, D. Xiao, Crystalline nickel boride nanoparticle agglomerates for enhanced electrocatalytic methanol oxidation, Int. J. Hydrogen Energy. 44 (2019) 23074–23080. https://doi.org/10.1016/j.ijhydene.2019.07.064.

[15] Y. Liu, H. Guo, K. Sun, J. Jiang, Magnetic CoOx@C-Reduced graphene oxide composite with catalytic activity towards hydrogen generation, Int. J. Hydrogen Energy. 44 (2019) 28163–28172. https://doi.org/10.1016/j.ijhydene.2019.09.034.

[16] Z. Chen, Q. Kang, G. Cao, N. Xu, H. Dai, P. Wang, Study of cobalt boride-derived electrocatalysts for overall water splitting, Int. J. Hydrogen Energy. 43 (2018) 6076–6087. https://doi.org/10.1016/j.ijhydene.2018.01.161.

[17] R. Fernandes, N. Patel, A. Miotello, M. Filippi, Studies on catalytic behavior of Co-Ni-B in hydrogen production by hydrolysis of NaBH4, J. Mol. Catal. A Chem. 298 (2009) 1–6. https://doi.org/10.1016/j.molcata.2008.09.014.

[18] J.C. Walter, A. Zurawski, D. Montgomery, M. Thornburg, S. Revankar, Sodium borohydride hydrolysis kinetics comparison for nickel, cobalt, and ruthenium boride catalysts, J. Power Sources. 179 (2008) 335–339. https://doi.org/10.1016/j.jpowsour.2007.12.006.

[19] N. Patel, R. Fernandes, A. Miotello, Promoting effect of transition metal-doped Co-B alloy catalysts for hydrogen production by hydrolysis of alkaline NaBH4 solution, J. Catal. 271 (2010) 315–324. https://doi.org/10.1016/j.jcat.2010.02.014.

[20] H. Li, Y. Wu, J. Zhang, W. Dai, M. Qiao, Liquid phase acetonitrile hydrogenation to ethylamine over a highly active and selective Ni-Co-B amorphous alloy catalyst, Appl. Catal. A Gen. 275 (2004) 199–206. https://doi.org/10.1016/j.apcata.2004.07.034.

[21] J.C. Ingersoll, N. Mani, J.C. Thenmozhiyal, A. Muthaiah, Catalytic hydrolysis of

sodium borohydride by a novel nickel-cobalt-boride catalyst, J. Power Sources. 173 (2007) 450–457. https://doi.org/10.1016/j.jpowsour.2007.04.040.

[22] J.H. Shen, Y.W. Chen, Catalytic properties of bimetallic NiCoB nanoalloy catalysts for hydrogenation of p-chloronitrobenzene, J. Mol. Catal. A Chem. 273 (2007) 265–276. https://doi.org/10.1016/j.molcata.2007.04.015.

[23] D. Xu, H. Wang, Q. Guo, S. Ji, Catalytic behavior of carbon supported Ni-B, Co-B and Co-Ni-B in hydrogen generation by hydrolysis of KBH4, Fuel Process. Technol. 92 (2011) 1606–1610. https://doi.org/10.1016/j.fuproc.2011.04.006.

[24] C. Wu, Y. Bai, D.X. Liu, F. Wu, M.L. Pang, B.L. Yi, Ni-Co-B catalyst-promoted hydrogen generation by hydrolyzing NaBH 4 solution for in situ hydrogen supply of portable fuel cells, Catal. Today. 170 (2011) 33–39. https://doi.org/10.1016/j.cattod.2011.01.046.

[25] S. Qiu, J. Huang, F. Shen, R. Pang, H. Chu, Y. Zou, C. Xiang, F. Xu, Y. Du, J. Wang, L. Sun, H. Zhou, Ternary Co–Ni–B amorphous alloy with a superior electrochemical performance in a wide temperature range, Int. J. Hydrogen Energy. 41 (2016) 3955–3960. https://doi.org/10.1016/j.ijhydene.2016.01.020.

[26] H. Euchner, P.H. Mayrhofer, Designing thin film materials-Ternary borides from first principles, Thin Solid Films. 583 (2015) 46–49. https://doi.org/10.1016/j.tsf.2015.03.035.

[27] A. Rinaldi, M.A. Correa-Duarte, V. Salgueirino-Maceira, S. Licoccia, E. Traversa, A.B. Dávila-Ibáñez, P. Peralta, K. Sieradzki, Elastic properties of hard cobalt boride composite nanoparticles, Acta Mater. 58 (2010) 6474–6486. https://doi.org/10.1016/j.actamat.2010.08.009.

[28] Y.P. Wang, Y.J. Wang, Q.L. Ren, L. Li, L.F. Jiao, D.W. Song, G. Liu, Y. Han, H.T. Yuan, Ultrafine amorphous Co-Fe-B catalysts for the hydrolysis of NaBH4 solution to

generate hydrogen for PEMFC, Fuel Cells. 10 (2010) 132–138. https://doi.org/10.1002/fuce.200900091.

[29] L. Li, Y.J. Wang, Y.P. Wang, Q.L. Ren, L.F. Jiao, H.T. Yuan, Effect of Ni content in Co1-xNixB catalysts on hydrogen generation during hydrolysis, Wuli Huaxue Xuebao/ Acta Phys. - Chim. Sin. 26 (2010) 1575–1578. https://doi.org/10.3866/PKU.WHXB20100609.

[30] Y. Zhao, L. Jiao, Y. Liu, L. Guo, L. Li, H. Liu, Y. Wang, H. Yuan, A synergistic effect between nanoconfinement of carbon aerogels and catalysis of CoNiB nanoparticles on dehydrogenation of LiBH4, Int. J. Hydrogen Energy. 39 (2014) 917–926. https://doi.org/10.1016/j.ijhydene.2013.10.137.

[31] S. Khoshsima, Z. Altıntaş, M. Schmidt, M. Bobnar, M. Somer, Ö. Balcı, Crystalline Co - Fe - B nanoparticles : Synthesis , microstructure and magnetic properties, 805 (2019). https://doi.org/10.1016/j.jallcom.2019.07.079.

[32] S. Khoshsima, Z. Altıntas, U. Burkhardt, M. Schmidt, K.G. Prashanth, M. Somer, Ö. Balcı, CoB-TiB 2 crystalline powders : Synthesis , microstructural analysis and their utilization as reinforcement agent, 31 (2020) 2964–2972. https://doi.org/10.1016/j.apt.2020.05.026.

[33] G. Gouget, D.P. Debecker, A. Kim, G. Olivieri, J.J. Gallet, F. Bournel, C. Thomas, O. Ersen, S. Moldovan, C. Sanchez, S. Carenco, D. Portehault, In Situ Solid-Gas Reactivity of Nanoscaled Metal Borides from Molten Salt Synthesis, Inorg. Chem. 56 (2017) 9225–9234. https://doi.org/10.1021/acs.inorgchem.7b01279.

[34] D. Portehault, S. Devi, P. Beaunier, C. Gervais, C. Giordano, C. Sanchez, M. Antonietti, A general solution route toward metal boride nanocrystals, Angew. Chemie - Int. Ed. 50 (2011) 3262–3265. https://doi.org/10.1002/anie.201006810.

[35] S. Guo, Q. Wu, J. Sun, T. Chen, M. Feng, Q. Wang, Z. Wang, B. Zhao, W. Ding,

Highly stable and controllable CoB/Ni-foam catalysts for hydrogen generation from alkaline NaBH4 solution, Int. J. Hydrogen Energy. 42 (2017) 21063–21072. https://doi.org/10.1016/j.ijhydene.2017.07.033.

[36] R. Retnamma, A.Q. Novais, C.M. Rangel, Kinetics of hydrolysis of sodium borohydride for hydrogen production in fuel cell applications: A review, Int. J. Hydrogen Energy. 36 (2011) 9772–9790. https://doi.org/10.1016/j.ijhydene.2011.04.223.

[37] X. Yuan, C. Jia, X. Ding, Z. Ma, Effects of heat-treatment temperature on properties of Cobalt - Manganese - Boride as efficient catalyst toward hydrolysis of alkaline sodium borohydride solution, Int. J. Hydrogen Energy. 37 (2011) 995–1001. https://doi.org/10.1016/j.ijhydene.2011.03.064.

[38] E.B. Kalkan, S. Akbayrak, S. Özkar, Ruthenium(0) nanoparticles supported on nanohafnia: A highly active and long-lived catalyst in hydrolytic dehydrogenation of ammonia borane, Mol. Catal. 430 (2017) 29–35. https://doi.org/10.1016/j.molcata.2016.11.042.

[39] Y. Tonbul, S. Akbayrak, S. Özkar, Palladium(0) nanoparticles supported on ceria: Highly active and reusable catalyst in hydrogen generation from the hydrolysis of ammonia borane, Int. J. Hydrogen Energy. 41 (2016) 11154–11162. https://doi.org/10.1016/j.ijhydene.2016.04.058.

[40] N. Patel, A. Miotello, Progress in Co-B related catalyst for hydrogen production by hydrolysis of boron-hydrides: A review and the perspectives to substitute noble metals, Int. J. Hydrogen Energy. 40 (2015) 1429–1464. https://doi.org/10.1016/j.ijhydene.2014.11.052.

[41] J. Li, X. Hong, Y. Wang, Y. Luo, P. Huang, B. Li, K. Zhang, Y. Zou, L. Sun, F. Xu, F. Rosei, S.P. Verevkin, A.A. Pimerzin, Encapsulated cobalt nanoparticles as a

recoverable catalyst for the hydrolysis of sodium borohydride, Energy Storage Mater. 27 (2020) 187–197. https://doi.org/10.1016/j.ensm.2020.01.011.

[42] J. Guo, Y. Hou, B. Li, Y. Liu, Novel Ni–Co–B hollow nanospheres promote hydrogen generation from the hydrolysis of sodium borohydride, Int. J. Hydrogen Energy. 43 (2018) 15245–15254. https://doi.org/10.1016/j.ijhydene.2018.06.117.

[43] R. Fernandes, N. Patel, A. Miotello, R. Jaiswal, D.C. Kothari, Stability, durability, and reusability studies on transition metal-doped Co-B alloy catalysts for hydrogen production, Int. J. Hydrogen Energy. 36 (2011) 13379–13391. https://doi.org/10.1016/j.ijhydene.2011.08.021.

[44] A. Didehban, M. Zabihi, N. Babajani, Preparation of the efficient nano-bimetallic cobalt-nickel catalysts supported on the various magnetic substrates for hydrogen generation from hydrolysis of sodium borohydride in alkaline solutions, Polyhedron. 180 (2020) 114405. https://doi.org/10.1016/j.poly.2020.114405.

[45] X. Wang, J. Liao, H. Li, H. Wang, R. Wang, B.G. Pollet, S. Ji, Highly active porous Co–B nanoalloy synthesized on liquid-gas interface for hydrolysis of sodium borohydride, Int. J. Hydrogen Energy. 43 (2018) 17543–17555. https://doi.org/10.1016/j.ijhydene.2018.07.147.

[46] S.C. Amendola, S.L. Sharp-Goldman, M.S. Janjua, M.T. Kelly, P.J. Petillo, M. Binder, An ultrasafe hydrogen generator: Aqueous, alkaline borohydride solutions and Ru catalyst, ACS Div. Fuel Chem. Prepr. 44 (1999) 864–866.

[47] H.Y. Kao, C.C. Lin, C.J. Hung, C.C. Hu, Kinetics of hydrogen generation on NaBH4 powders using cobalt catalysts, J. Taiwan Inst. Chem. Eng. 87 (2018) 123–130. https://doi.org/10.1016/j.jtice.2018.03.022.

[48] Y. Wang, K. Zou, D. Zhang, Z. Cao, K. Zhang, Y. Xie, Gong zhou, G. Li, S. Bai, Cobalt–copper–boron nanoparticles as catalysts for the efficient hydrolysis of alkaline

sodium borohydride solution, Int. J. Hydrogen Energy. 45 (2020) 9845–9853. https://doi.org/10.1016/j.ijhydene.2020.01.157.

[49] Y. Wei, W. Meng, Y. Wang, Y. Gao, K. Qi, K. Zhang, Fast hydrogen generation from NaBH4 hydrolysis catalyzed by nanostructured Co–Ni–B catalysts, Int. J. Hydrogen Energy. 42 (2017) 6072–6079. https://doi.org/10.1016/j.ijhydene.2016.11.134.

[50] S. Gupta, M.K. Patel, A. Miotello, N. Patel, Metal Boride-Based Catalysts for Electrochemical Water-Splitting: A Review, Adv. Funct. Mater. 30 (2020). https://doi.org/10.1002/adfm.201906481.

[51] L. Wang, M. Zhong, J. Li, X. Zhao, W. Hao, Y. Guo, Highly efficient ferromagnetic Co–B–O catalyst for hydrogen generation, Int. J. Hydrogen Energy. 43 (2018) 17164–17171. https://doi.org/10.1016/j.ijhydene.2018.07.107.